Editorial

Advances in super-resolution photoacoustic imaging

Junhui Shi[1], Yuqi Tang[2], Junjie Yao[2]

[1]Caltech Optical Imaging Laboratory, Andrew and Peggy Cherng Department of Medical Engineering, Department of Electrical Engineering, California Institute of Technology, Pasadena, CA 91125, USA; [2]Photoacoustic Imaging Laboratory, Department of Biomedical Engineering, Duke University, Durham, NC 27708, USA

Correspondence to: Junjie Yao. Photoacoustic Imaging Laboratory, Department of Biomedical Engineering, Duke University, Durham, NC 27708, USA. Email: junjie.yao@duke.edu.

Submitted Sep 09, 2018. Accepted for publication Sep 17, 2018.
doi: 10.21037/qims.2018.09.14
View this article at: http://dx.doi.org/10.21037/qims.2018.09.14

Introduction

Photoacoustic (PA) imaging (PAI), or optoacoustic imaging, is a hybrid imaging modality that combines optical absorption contrast and ultrasound image formation. In PAI, the target is excited by a short laser pulse and subsequently absorbs the photon energy, leading to a transient local temperature rise. The temperature rise induces a local pressure rise that propagates as acoustic waves. As acoustic waves generally undergo less scattering and attenuation in tissue compared with light, PAI can provide high-resolution images in both the optical (quasi)ballistic and (quasi)diffusive regimes (1,2). Based on the image formation methods, PAI can be classified into two categories: photoacoustic microscopy (PAM) and photoacoustic computed tomography (PACT). PAM uses a focused excitation light beam and/or a focused single-element ultrasonic transducer for direct image formation through position scanning (1,2). PAM has a maximum imaging depth ranging from a few hundred micrometers to a few millimeters with spatial resolution ranging from sub-micrometer to sub-millimeter (2,3). PAM can be further classified into optical-resolution PAM (OR-PAM) and acoustic-resolution PAM (AR-PAM). For both OR-PAM and AR-PAM, the axial resolution is determined by the bandwidth of the ultrasonic transducer (4). OR-PAM works in the optical (quasi)ballistic regime, whereas the light is tightly focused that it can penetrate about one optical transport mean free path (~1 mm in soft tissue). Therefore, the lateral resolution of OR-PAM is mainly determined by the optical focal spot size (4-6). The optical focusing is diffraction-limited as $\lambda/2NA$, where λ is the light wavelength, and NA is the numerical aperture of objective lens. On the contrary, in AR-PAM, the laser is loosely focused to fulfill the entire acoustic focal spot, thereby penetrating a few optical transport mean free paths, i.e., in the quasi-diffusive regime. The lateral resolution of AR-PAM is thus determined by the size of acoustic focus (4,7,8), limited by acoustic diffraction. In PACT, the object is illuminated with a wide-field laser beam in the diffusive regime, and the generated acoustic waves are detected at multiple locations or by using a multi-element transducer array. The image formed by PACT is reconstructed by an inverse algorithm. The spatial resolution of PACT is fundamentally limited by acoustic diffraction, and additionally affected by the directionality and spacing of the detector elements (9).

Recently, several studies have shown that sub-diffraction imaging of biological samples can be achieved through PAI by breaking optical-diffraction limit in the (quasi) ballistic regime or acoustic-diffraction limit in the (quasi) diffusive regime, which have opened new possibilities for fundamental biological studies. Yao *et al.* developed a photoimprint PAM using the intensity-dependent photobleaching effect and acquired a melanoma cell PA image with a lateral resolution of 90 nm (10). Danielli *et al.* reported a label-free PA nanoscopy based on the optical-absorption saturation effect and acquired a mitochondria PA image with a lateral resolution of 88 nm (11). Chaigne *et al.* exploited the sample-dynamics-induced inherent temporal fluctuation in the PA signals and achieved a resolution enhancement of about 1.4 over conventional

PACT (12). Murray *et al.* broke the acoustic diffraction limit by implementing a blind speckle illumination and block-FISTA reconstruction algorithm and achieved a resolution close to the acoustic speckle size (13). Dean-Ben *et al.* also overcame the acoustic diffraction limit by incorporating rapid sequential acquisition of 3D PA images of flowing absorbing particles and further enhanced the visibility of structures under limited-view tomographic conditions (14). Conkey *et al.* optimized wavefront shaping with photoacoustic feedback and achieved up to ten times improvement in signal-to-noise ratio and five to six times sub-acoustic-diffraction resolution (15). In this concise review, we summarize and analyze the recent development in super-resolution (SR) PAI (SR-PAI) in both the optical (quasi)ballistic and (quasi)diffusive regime, as well as their representative applications. We also discuss the current challenges in SR-PAI and envision the potential breakthroughs.

Super-resolution OR-PAM in (quasi)ballistic regime

For OR-PAM of biological tissue at relatively superficial region, typically within one mean free path of optical scattering (<1 mm), the light propagation is in the optical (quasi)ballistic regime. Within this range, the light beam can be tightly focused on the target, and the lateral resolution is determined by the optical focal spot size, which is limited by optical diffraction, similar to other traditional optical imaging methods (16-18). To achieve super-resolution OR-PAM in the (quasi)ballistic regime, two strategies based on nonlinear optical mechanisms have been successfully exploited to overcome the optical diffraction limit (10,11).

The first strategy is reported by Yao *et al.*, who developed photoimprint PAM (PI-PAM) based on the intensity-dependent photobleaching effect (19). Dual-pulse excitation process was implemented in this method, and its principle is illustrated in *Figure 1A*. The first excitation generates a PA signal from the whole excitation volume, and at the same time, bleaches more absorbers in the central diffraction-limited excitation volume than those in the peripheral region, due to the inherent illumination inhomogeneity of a Gaussian beam. In the subsequent second excitation, molecules in the bleached central area have reduced absorption and generate a smaller PA signal than that from the first excitation. Although the PA signals generated from the two excitations are linear to the excitation energy, the difference between the two PA signals, which mostly represents the signal contribution from the central area of the focus, is nonlinear to the excitation energy. This mechanism of nonlinearity endows PI-PAM with both lateral and axial resolution enhancement, and the resultant imaging resolution is determined by the 'sharpened' focal spot. Compared to the diffraction-limited PAM, the lateral resolution of PI-PAM is enhanced by a factor of $\sqrt{1+b}$, where b is the power dependence of the photobleaching rate on the excitation intensity. In addition, the axial resolution of PI-PAM is improved by a factor of $1/\sqrt{2^{1(1+b)}-1}$ over conventional PAM. *Figure 1B,C* show the lateral resolution enhancement of PI-PAM over conventional OR-PAM. This imaging method can be performed on both fluorescent and nonfluorescent biological species. The major drawback of this method is the potential sample damage due to inherent photobleaching. The high frame number or excitation intensity may result in severe distortion between 'bleached' and 'unbleached' regions, thus balancing between sample distortion and SNR needs to be carefully sought. In practice, permanent photobleaching might become a concern, and photoswitchable chromophores can be introduced and cycled between bright and dark state (10,20,21). Moreover, different samples may have inconsistent resolution enhancement due to their different power dependence of photobleaching rates on the light intensity.

The second strategy attains nonlinear SR-PAM by using nonlinear thermal expansion and optical absorption saturation (11). The magnitude of PA signal is proportional to thermal expansion coefficient $\beta(T)$, which is temperature dependent. When T is in the physiological temperature range, $\beta(T)\approx\beta_1+\beta_2 T$ (22). For typical biological tissues with a nanosecond laser pulse excitation, the thermal diffusion length is around tens of nanometer (23). On the other hand, the optical excitation spot is around hundreds of nanometers, which is confined by the optical diffraction limit. Therefore, there exists the nonlinear enhancement of PA signals due to the local temperature rise within a short-pulsed optical excitation. In addition, the optical absorption coefficient saturates with increasing optical fluence (24), thereby contributing a second source of nonlinearity to the PA signals. Based on these two effects, high order nonlinear PA images can be constructed by using an optical pulse train with different energies striking on the same target. Given M optical pulses in a train, PA images with up to Nth-order

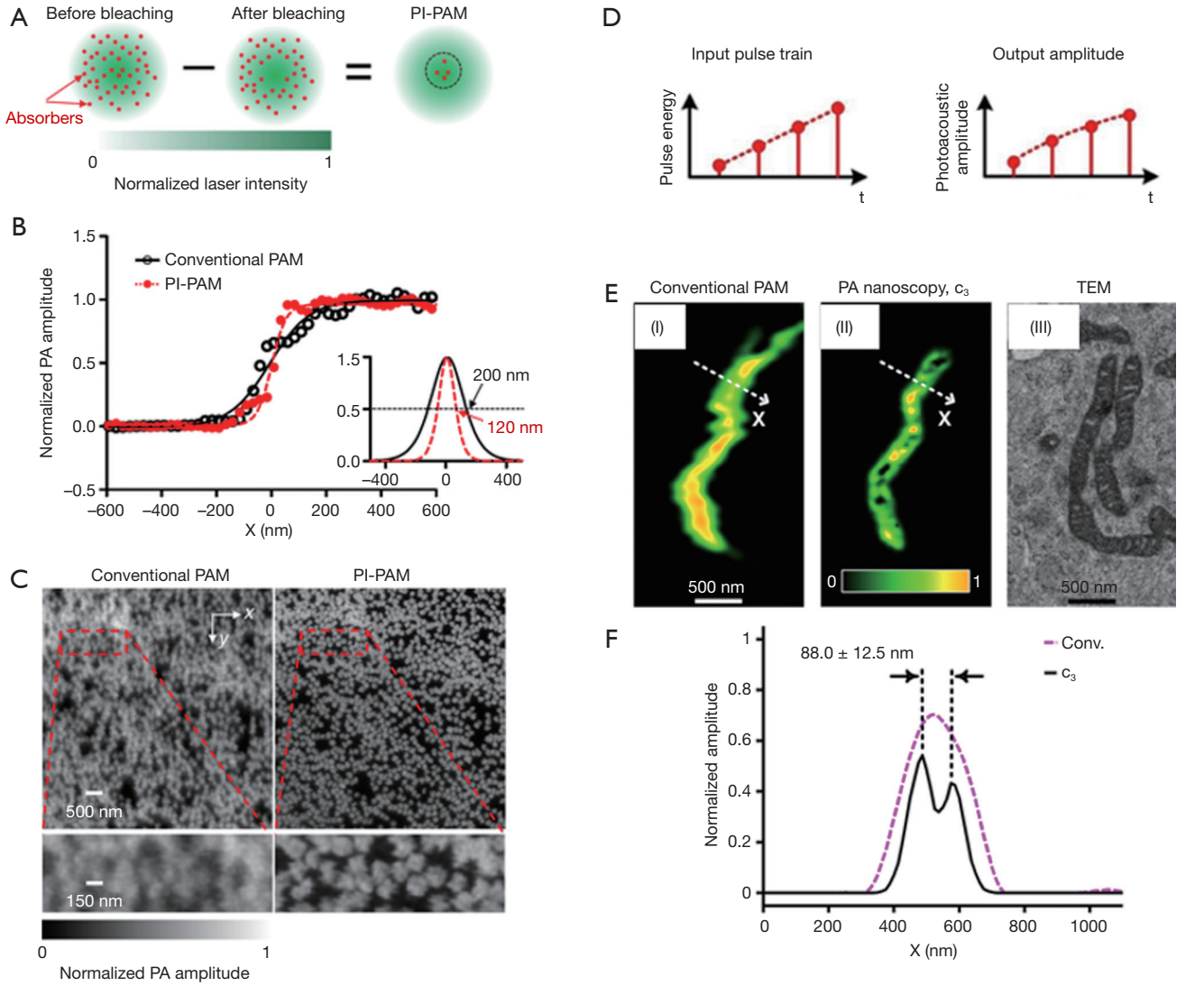

Figure 1 Two methods of nonlinear OR-PAM with sub-diffraction resolution. (A) Principle of PI-PAM; (B) the edge spread function of PI-PAM and conventional OR-PAM. The lateral resolution is improved from 200 to 120 nm; (C) comparison of images of red-dyed microspheres obtained by conventional PAM and PI-PAM, showing the improved lateral resolutions; (D) principle of nonlinear-absorption based PA-nanoscopy; (E) images of a single mitochondrion obtained by conventional PAM and PA-nanoscopy, which resolves 88-nm-apart features; (F) signal profiles along the dashed lines in (E), showing the improved resolution of PA-nanoscopy. Figure adopted with permission from (10,11). OR-PAM, optical-resolution photoacoustic microscopy; PI-PAM, photoimprint photoacoustic microscopy.

(N≤M) can be formed. The nonlinear high-order PA image narrows the lateral point spread function (PSF), thereby improves the lateral resolution by a factor of $\sqrt{N}$ over that of conventional PAM. In Danielle *et al.*'s work (11), a train of 1.6-ns laser pulses with pulse-to-pulse intensity modulation was used to embody this method. As illustrated in *Figure 1D*, at each position, four PA signals are successively excited with increasing pulse energy, then the third-order PA signals are extracted to achieve sub-diffraction resolution. In the experiment demonstration of this method, it reveals 88-nm features in a single mitochondrion (*Figure 1E,F*). The major drawbacks of this method include the long imaging time, slow pixel-by-pixel high-order fitting, and potential heating and photobleaching damage to the sample with repeated

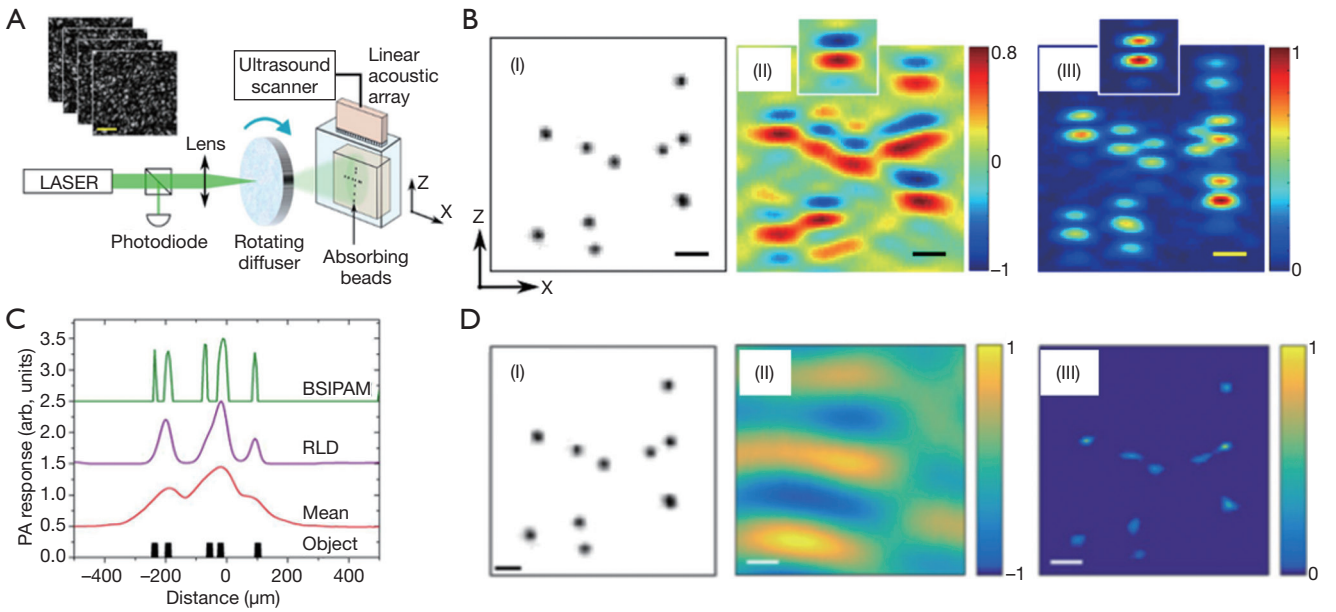

Figure 2 Sub-acoustic-diffraction PA imaging based on statistical fluctuation of PA signals and blind speckle illumination. (A) Experimental setup of fluctuation PA imaging with multiple speckle illumination. The blind-speckle illumination PAM has a similar scheme; (B) photography of sample (left), mean PA image over 100 speckle realizations (middle), and variance PA image (right). Figures adopted with permission from (25); (C) 1D demonstration with blind-speckle illumination PAM. Figures adopted with permission from (13); (D) a 2D image (right) obtained by blind-speckle illumination PAM, compared to photography of sample (left), mean PA image (middle). Figures adopted with permission from (26). PA, photoacoustic; PAM, photoacoustic microscopy.

excitation. Though no observable damages were reported on *ex vivo* cells, shorter pulses with lower energy can be used to approach the saturation intensity level with reduced photothermal damage potential (11).

Super-resolution PA imaging in (quasi)diffusive regime

For deep tissue imaging, it is challenging to focus light at depths beyond the optical mean free path (i.e., >1 mm). As light enters the (quasi)diffusive regime, the acoustic diffraction determines the lateral resolution of AR-PAM and PACT. To break the acoustic diffraction limit, several techniques have been exploited by probing the PA signal fluctuation (12,25), deconvolution with speckle structure illumination (13,26), localization of flowing absorbing particles (14,27), and improving optical focusing through wavefront shaping (15).

Originally developed for improving the resolution of conventional fluorescence microscopy, the statistical analysis of temporal signal fluctuations provides a simple way to obtain sub-diffraction optical resolution (28). Inspired by this approach, Chaigne *et al.* reported two similar methods (12,25) to achieve SR-PAI using temporal PA signal fluctuation analysis. The first method introduced multiple optical speckle illumination as the source of signal fluctuations (25). Since the speckle grain size was smaller than the acoustic focal spot size, a sub-diffraction acoustic resolution image was formed from analyzing second-order fluctuation of PA images with a number of random speckle illumination patterns. As illustrated in *Figure 2A,B*, this method achieved a resolution enhancement of about 1.4 times over conventional PACT. The second method relies on the fluctuation analysis of varying PA signals induced by flowing absorbing particles (12). With the natural motion of flowing particles, the fluctuation-analysis-based method is further simplified, and a long-coherence laser focus is no longer required for deep-tissue speckle illumination as in the first method. The second method can achieve a $\sqrt{n}$ resolution enhancement using n^{th}-order cumulant analysis. Nevertheless, the fluctuation-based methods are slow and likely to suffer from the natural motion artifacts for *in vivo*

applications, including the heart beating and breathing.

Inspired by blind speckle illumination in super-resolution fluorescence imaging, Murray *et al.* implemented this method to break the acoustic diffraction limit in PAI in scattering media (13,29). Encoded with unknown speckle illumination patterns, the generated PA image is a convolution of the system's PSF and the spatial product of speckle pattern and absorber distribution. Although the PA image reconstruction using this scheme is an ill-conditioned deconvolution process with a smooth kernel, Murray *et al.* assumed block sparsity and developed an efficient deconvolution algorithm called block-FISTA (fast iterative shrinkage-thresholding algorithm) to obtain high-resolution images. The PAT setup is similar to the fluctuation-analysis based method with speckle illumination. The experimental demonstration in *Figure 2C* clearly showed that this method has a much better resolution than the regular deconvoluted or averaged PA images. The 2D image formation (*Figure 2D*) with this method was also realized with a linear transducer array in an independent study by Hojman *et al.* (26).

Localization of sub-diffraction absorbers is the basis of stochastic super-resolution fluorescence microscopy (30,31), which has enabled *in vivo* sub-cellular biochemical research since 2006. The super-resolution localization images are constructed by superposition of a large number of isolated individual sources, which are otherwise not resolvable due to the diffraction limit. In the past two years, localization-based super-resolution ultrasound imaging has also been achieved through tracking microbubbles in deep vessels (32). Recently, two independent studies overcame the acoustic diffraction limit in PAI by localizing flowing optical absorbers (14,27). Vilov *et al.* performed a proof-of-principle experiment using microbeads flowing in microfluidic channels and imaged by a 15-MHz linear transducer array (27), while Dean-Ben *et al.* demonstrated 3D imaging of a knotted pipette filled with flowing microbeads imaged by a 4 MHz semi-spherical transducer array (14). In both studies, sparsely distributed PA point sources, i.e., microbeads, were driven through the micro-tubing or micro-channels and repeatedly captured in sequential PA images. The localization images were constructed through superposition of the central positions of point sources extracted from each PA image (*Figure 3A,B,C*). While the point sources were blurred in each conventional PA images due to acoustic diffraction limit, the localization image was able to break this limit and achieve sub-diffraction resolution (16,33). Nevertheless, the concept has only been demonstrated on simple phantoms without background signals or motion artifacts, and its applications for animal studies are expected to be more challenging due to reduced signal strength and image contrast.

Another way to achieve SR-PAI in deep tissue is to create a sub-acoustic-diffraction optical focus through optical wavefront shaping. Focusing light in highly scattering media has long been sought for deep-tissue imaging at optical resolution (34-37). Most of the reported wavefront shaping techniques rely on a guide-star inside the media to provide optical signal feedback (e.g., fluorescence, transmittance) for wavefront optimization. Similarly, Conkey *et al.* optimized optical wavefront using PA signals as the feedback (15). As illustrated in *Figure 3D*, the optical speckle pattern inside the ultrasound focal region was optimized using PA signal feedback through evolution algorithm, and finally reached sub-acoustic-diffraction optical focusing. When scanning the object with the optimized optical focusing, 2D PA images with sub-acoustic-diffraction resolution are formed. Using this method, Conkey *et al.* demonstrated a 13 μm resolution, which is much better than the conventional PAI (*Figure 3E*), but the speed for optimization and scanning was low. In future, with the advances in optical components and optimization algorithms, wavefront shaping in scattering media will be improved in its speed and robustness for SR-PAI in deep tissue.

Conclusions

In this concise review, we summarized various SR-PAI methods that have been explored to improve the resolution finer than either the optical or acoustic diffraction. *Table 1* lists these methods and compares their mechanisms, key performance, strength and weakness. The technological advances in SR-PAI have opened new possibilities for fundamental biological studies. Compared with conventional fluorescence-based super-resolution microscopy, SR-PAI is label-free and thus can minimize the possibility of introducing image artefacts during the labeling process (38). While other label-free imaging technologies such autofluorescence-based and phase-sensitive microscopy are limited to thin samples or superficial tissues (11,39,40), SR-PAI can provide functional and structural information by imaging endogenous chromophores (e.g., hemoglobin, melanin, lipids, DNA/RNA) or exogenous chromophores (e.g., nanoparticles, organic dyes, reporter gene products) at depths far beyond the optical diffusion limit (41). Mostly

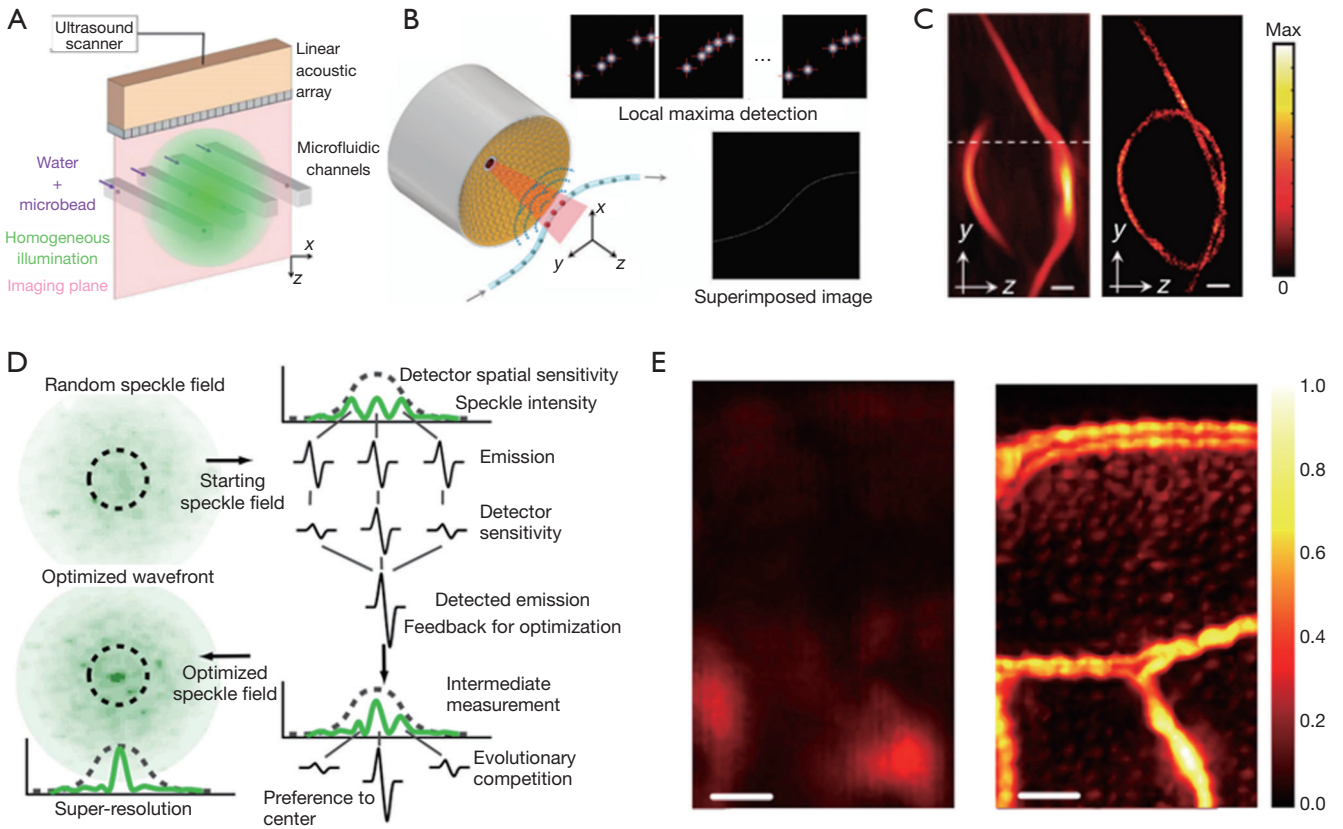

Figure 3 Sub-acoustic-diffraction PA imaging based on particle localization and wavefront shaping. (A,B) The experimental setup of localization PA imaging with a linear array (A) (27) and semi-spherical array (B) (14); (C) images of a knotted pipette tip (~220 μm in diameter) obtained by conventional PACT (left) and localization PA imaging (right). Scale bar: 600 μm. Figures adopted with permission from (14,27); (D) the principle of optical focusing in highly scattering media by wavefront shaping with PA feedback; (E) images of a sweat bee wing obtained by conventional AR-PAM (left) and PAM with optical focusing through wavefront shaping (right). Scale bar: 100 μm. Figures adopted with permission from (15). PA, photoacoustic; PACT, photoacoustic computed tomography; AR-PAM, acoustic-resolution photoacoustic microscopy.

excitingly, the novel AR-PAM and PACT technologies with finer resolutions than the acoustic diffraction can potentially benefit *in vivo* cancer diagnostics, hemodynamics studies, and neuroscience research.

Nevertheless, challenges largely remain for deep-tissue SR-PAI. Applying blind illumination for deep tissue imaging is difficult because of the large difference between the optical speckle grain dimensions and the acoustic focal spot size. Longer optical wavelengths and higher ultrasound frequency will be beneficial to overcome the difficulty in the future (26). In optical wavefront shaping, the greatest challenge is to focus the light inside the living biological tissue with fast decorrelation motions such as blood flow and breathing. The number of input modes and genetic algorithm iterations need to be decreased, at the price of focusing quality (15). To detect PA signal fluctuation induced by flowing particles, the number of characteristic images may limit the temporal resolution of the technique (12,25,42). Similarly, the time for localizing absorbing particles depends on the frame rate and the number of pixels per image. The temporal resolution can be optimized by increasing the particle density, but it is still challenging for real-time imaging (14). Future improvements in the SR-PAI methods are needed and more phantom and *in vivo* validations should be performed to strengthen these methods.

Table 1 Summary of methods used for SR-PAI

Depth regime	Imaging modality	Mechanism	Resolution		Imaging speed	Pros	Cons	Ref
			Lateral	Axial				
Ballistic	OR-PAM	Nonlinear photobleaching effect	90 nm	400 nm	Medium	Can be applied to both fluorescent and nonfluorescent samples. Capable of optical sectioning	The high frame number or excitation intensity may result in severe distortion between 'bleached' and 'unbleached' regions	(10)
		Nonlinear absorption coefficient	88 nm	–	Medium	High-order PA image leads to higher resolution. Capable of optical sectioning	Long imaging time, slow pixel-by-pixel high-order fitting, and potential heating and photobleaching damage to the sample with repeated excitation	(11)
Diffusive	AR-PAM	Deconvolution with blind speckle illumination	80 μm	–	Low	Uses blind structure illumination to achieve F imaging. Efficiently exploits dynamic temporal fluctuations	Requires sparsity of the structures The small fluctuations over a large background may be challenging under low SNR conditions	(13,26)
		Improved optical focus through wavefront shaping	30 μm	–	Low	Can create an optical focal spot five times smaller than the acoustic focal spot size in scattering medium	Feedback optimization of wavefront for each pixel is very slow	(15)
	PACT (OAT)	Photoacoustic signal fluctuation induced by flowing particles	72 μm	–	Low	Free from common photoacoustic imaging artifacts caused by band-limited acoustic detection. Potential for label-free microvessel imaging	Lacks high temporal resolution intrinsically. Requires high frame rate for fluctuation analysis	(12)
		Photoacoustic signal fluctuation with multiple speckle illumination	160 μm	–	Low	Simple experimental setup. Reveals high spatial frequencies by considering fluctuations in PA images	Requires a very large number of frames for high SNR	(25)
		Localization of flowing absorbing particles	78 μm	112 μm	Very low	Not affected by flow rate. Enhances the visibility of structures under limited-view conditions	Needs high frame rate and high particle density	(14,27)

SR-PAI, super-resolution photoacoustic imaging; OR-PAM, optical-resolution photoacoustic microscopy; AR-PAM, acoustic-resolution photoacoustic microscopy; PACT, photoacoustic computed tomography; SNR, signal-to-noise ratio.

Acknowledgements

Funding: We would like to thank the support from Duke MEDx Basic Science Pilot Grant, Duke Center for Genomic and Computational Biology Faculty Pilot Research Grant, and American Heart Association Collaborative Sciences Award 18CSA34080277 (all to J Yao).

Footnote

Conflicts of Interest: The authors have no conflicts of interest to declare.

References

1. Xia J, Yao J, Wang LV. Photoacoustic tomography: principles and advances. Electromagn Waves (Camb) 2014;147:1-22.
2. Wang LV. Multiscale photoacoustic microscopy and computed tomography. Nat Photonics 2009;3:503-9.
3. Wang LV, Hu S. Photoacoustic tomography: in vivo imaging from organelles to organs. Science 2012;335:1458-62.
4. Yao J, Wang LV. Photoacoustic microscopy. Laser Photon Rev 2013;7:758-78.
5. Hu S, Maslov K, Wang LV. Second-generation optical-resolution photoacoustic microscopy with improved sensitivity and speed. Opt Lett 2011;36:1134-6.
6. Maslov K, Zhang HF, Hu S, Wang LV. Optical-resolution photoacoustic microscopy for in vivo imaging of single capillaries. Opt Lett 2008;33:929-31.
7. Zhang HF, Maslov K, Stoica G, Wang LV. Functional photoacoustic microscopy for high-resolution and noninvasive in vivo imaging. Nat Biotechnol 2006;24:848-51.
8. Maslov K, Stoica G, Wang LV. In vivo dark-field reflection-mode photoacoustic microscopy. Opt Lett 2005;30:625-7.
9. Cox B, Laufer JG, Beard PC, Arridge SR. Quantitative spectroscopic photoacoustic imaging: a review. J Biomed Opt 2012;17:061202.
10. Yao J, Wang L, Li C, Zhang C, Wang LV. Photoimprint photoacoustic microscopy for three-dimensional label-free subdiffraction imaging. Phys Rev Lett 2014;112:014302.
11. Danielli A, Maslov KI, Garcia-Uribe A, Winkler AM, Li C, Wang L, Chen Y, Dorn GW, Wang LV. Label-free photoacoustic nanoscopy. J Biomed Opt 2014;19:086006.
12. Chaigne T, Arnal B, Vilov S, Bossy E, Katz O. Super-resolution photoacoustic imaging via flow-induced absorption fluctuations. Optica 2017;4:1397-404.
13. Murray TW, Haltmeier M, Berer T, Leiss-Holzinger E, Burgholzer P. Super-resolution photoacoustic microscopy using blind structured illumination. Optica 2017;4:17-22.
14. Dean-Ben XL, Razansky D. Localization optoacoustic tomography. Light Sci Appl 2018;7:18004.
15. Conkey DB, Caravaca-Aguirre AM, Dove JD, Ju H, Murray TW, Piestun R. Super-resolution photoacoustic imaging through a scattering wall. Nat Commun 2015;6:7902.
16. Bower AJ, Chidester B, Li J, Zhao Y, Marjanovic M, Chaney EJ, Do MN, Boppart SA. A quantitative framework for the analysis of multimodal optical microscopy images. Quant Imaging Med Surg 2017;7:24-37.
17. Kam J, Zhang Q, Lin J, Liu J, Wang RK, Rezaei K. Optical coherence tomography based microangiography findings in hydroxychloroquine toxicity. Quant Imaging Med Surg 2016;6:178-83.
18. Le N, Song S, Zhang Q, Wang RK. Robust principal component analysis in optical micro-angiography. Quant Imaging Med Surg 2017;7:654-67.
19. Jacobson K, Elson E, Koppel D, Webb W. Fluorescence photobleaching in cell biology. Nature 1982;295:283.
20. Bates M, Huang B, Dempsey GT, Zhuang X. Multicolor super-resolution imaging with photo-switchable fluorescent probes. Science 2007;317:1749-53.
21. Subach OM, Patterson GH, Ting L-M, Wang Y, Condeelis JS, Verkhusha VV. A photoswitchable orange-to-far-red fluorescent protein, PSmOrange. Nat Methods 2011;8:771-7.
22. Larina IV, Larin KV, Esenaliev RO. Real-time optoacoustic monitoring of temperature in tissues. J Phys D Appl Phys 2005;38:2633.
23. Wang LV, Wu H. Biomedical optics: principles and imaging. John Wiley & Sons; 2012.
24. Siegman AE. Lasers university science books. Mill Valley, CA 1986;37:208.
25. Chaigne T, Gateau J, Allain M, Katz O, Gigan S, Sentenac A, Bossy E. Super-resolution photoacoustic fluctuation imaging with multiple speckle illumination. Optica 2016;3:54-7.
26. Hojman E, Chaigne T, Solomon O, Gigan S, Bossy E, Eldar YC, Katz O. Photoacoustic imaging beyond the acoustic diffraction-limit with dynamic speckle illumination and sparse joint support recovery. Opt Express 2017;25:4875-86.
27. Vilov S, Arnal B, Bossy E. Overcoming the acoustic diffraction limit in photoacoustic imaging by the localization of flowing absorbers. Opt Lett 2017;42:4379-82.
28. Dertinger T, Colyer R, Iyer G, Weiss S, Enderlein J. Fast, background-free, 3D super-resolution optical fluctuation imaging (SOFI). Proc Natl Acad Sci U S A 2009;106:22287-92.
29. Mudry E, Belkebir K, Girard J, Savatier J, Le Moal E, Nicoletti C, Allain M, Sentenac A. Structured illumination microscopy using unknown speckle patterns. Nat Photonics 2012;6:312-5.
30. Betzig E, Patterson GH, Sougrat R, Lindwasser OW, Olenych S, Bonifacino JS, Davidson MW, Lippincott-Schwartz J, Hess HF. Imaging intracellular fluorescent

proteins at nanometer resolution. Science 2006;313:1642-5.
31. Rust MJ, Bates M, Zhuang X. Sub-diffraction-limit imaging by stochastic optical reconstruction microscopy (STORM). Nat Methods 2006;3:793.
32. Errico C, Pierre J, Pezet S, Desailly Y, Lenkei Z, Couture O, Tanter M. Ultrafast ultrasound localization microscopy for deep super-resolution vascular imaging. Nature 2015;527:499.
33. Fehm TF, Deán-Ben XL, Ford SJ, Razansky D. In vivo whole-body optoacoustic scanner with real-time volumetric imaging capacity. Optica 2016;3:1153-9.
34. Vellekoop IM, Mosk A. Focusing coherent light through opaque strongly scattering media. Opt Lett 2007;32:2309-11.
35. Yaqoob Z, Psaltis D, Feld MS, Yang C. Optical phase conjugation for turbidity suppression in biological samples. Nat Photonics 2008;2:110.
36. Vellekoop IM, Lagendijk A, Mosk A. Exploiting disorder for perfect focusing. Nat Photonics 2010;4:320.
37. Bertolotti J, van Putten EG, Blum C, Lagendijk A, Vos WL, Mosk AP. Non-invasive imaging through opaque scattering layers. Nature 2012;491:232.
38. Huang B, Bates M, Zhuang X. Super-resolution fluorescence microscopy. Annu Rev Biochem 2009;78:993-1016.
39. Bierwagen J, Testa I, Fölling J, Wenzel D, Jakobs S, Eggeling C, Hell SW. Far-field autofluorescence nanoscopy. Nano Lett 2010;10:4249-52.
40. Cotte Y, Toy F, Jourdain P, Pavillon N, Boss D, Magistretti P, Marquet P, Depeursinge C. Marker-free phase nanoscopy. Nat Photonics 2013;7:113.
41. Beard P. Biomedical photoacoustic imaging. Interface Focus 2011;1:602-31.
42. Gateau J, Chaigne T, Katz O, Gigan S, Bossy E. Improving visibility in photoacoustic imaging using dynamic speckle illumination. Opt Lett 2013;38:5188-91.

Cite this article as: Shi J, Tang Y, Yao J. Advances in super-resolution photoacoustic imaging. Quant Imaging Med Surg 2018;8(8):724-732. doi: 10.21037/qims.2018.09.14

